
UNCERTAINTY-AWARE VARIATIONAL INFORMATION PURSUIT FOR INTERPRETABLE MEDICAL IMAGE ANALYSIS

Md Nahiduzzaman
School of Computing Technologies
RMIT University
Melbourne VIC 3000, Australia
s4045807@student.rmit.edu.au

Ruwan Tennakoon
School of Computing Technologies
RMIT University
Melbourne VIC 3000, Australia
ruwan.tennakoon@rmit.edu.au

Steven Korevaar
School of Computing Technologies
RMIT University
Melbourne VIC 3000, Australia
steven.korevaar@rmit.edu.au

Zongyuan Ge
Faculty of Engineering
Monash University
Clayton VIC 3800, Australia
zongyuan.ge@monash.edu

Alireza Bab-Hadiashar
School of Engineering
RMIT University
Melbourne VIC 3000, Australia
alireza.bab-hadiashar@rmit.edu.au

June 23, 2025

ABSTRACT

In medical imaging, AI decision-support systems must balance accuracy and interpretability to build user trust and support effective clinical decision-making. Recently, Variational Information Pursuit (V-IP) and its variants have emerged as interpretable-by-design modeling techniques, aiming to explain AI decisions in terms of human-understandable, clinically relevant concepts. However, existing V-IP methods overlook instance-level uncertainties in query-answer generation, which can arise from model limitations (epistemic uncertainty) or variability in expert responses (aleatoric uncertainty).

This paper introduces Uncertainty-Aware V-IP (UAV-IP), a novel framework that integrates uncertainty quantification into the V-IP process. We evaluate UAV-IP across four medical imaging datasets, PH2, Derm7pt, BrEaST, and SkinCon, demonstrating an average AUC improvement of approximately 3.2% while generating 20% more concise explanations compared to baseline V-IP, without sacrificing informativeness. These findings highlight the importance of uncertainty-aware reasoning in interpretable by design models for robust and reliable medical decision-making.

Keywords Interpretable models · interpretable-by-design · xAI · Explainable AI · Uncertainty · Variational Information Pursuit.

1 Introduction

In real-world applications such as medical imaging, AI decision support systems must be both accurate and interpretable to enable effective decision-making. While deep learning (DL) has demonstrated exceptional performance, its “black box” nature often diminishes user trust in its decisions [1, 2].

Early works to enhance the interpretability of DL in image classification focused on post-hoc (PH) techniques, such as saliency map-based methods, which aim to highlight the regions of an image most influential in the model’s decision [3, 4, 5]. PH techniques often do not offer human-like explanations (e.g. why a particular region was important, or how it contributes to the classification) and can sometimes lead to misleading or inaccurate interpretations [6, 7, 8].

In medical imaging, where humans typically make the final decisions, it is desirable to present AI system interpretations in clinically relevant terms. For example, when diagnosing a skin disease, the interpretations could refer to clinical features, such as “Is a blue-whitish veil present?” or “Is the lesion’s structure regular?”. The Concept Bottleneck

Models (CBM) [9, 10, 11] address this by first predicting human-understandable concepts and subsequently using these concepts to make final predictions. This provides an intermediary layer of interpretability. However, CBM-based methods assume that these concepts are linearly additive, an unrealistic assumption given that different concepts may not have a linear relationship with each other [12]. As a result, the Variational Information Pursuit (V-IP) [13, 14] model was recently introduced to mimic human-like decision-making through active testing [15]. In this framework, V-IP sequentially poses a set of queries (e.g., presence or absence of clinical concepts) to gather information about the input. Based on answers to each query provided by a learned model (e.g., CBM), V-IP updates its belief about the input image’s class. The explanation constitutes a minimal sequence of query-answer pairs needed to achieve a confident decision.

A key limitation of current V-IP-based models is their inability to account for sample-level uncertainties¹ in the generation of query answers². Since V-IP-based methods rely on a trained model that generates answers to queries, factors such as limited data availability and model complexity can result in epistemic or model uncertainty [16, 17]. Furthermore, in the medical domain, variability in expert responses often indicate aleatoric or data uncertainty [18, 17, 19]. Human decision-making often prioritizes more certain answers over uncertain ones. For example, if determining the concept “Is a blue-whitish veil present?” for a particular lesion is uncertain, a human expert may prioritize other more reliable concepts, whereas V-IP still incorporates it into the decision-making process.

This paper addresses this limitation in V-IP and introduces the Uncertainty Aware V-IP (UAV-IP) framework. Unlike prior work such as evi-CEM [20] and ProbCBM [21], which model concept uncertainty but still pass all concepts, regardless of their certainty into the classifier, thus uncertainty is only used implicitly, and may be underutilized. UAV-IP explicitly uses uncertainty to filter out unreliable concepts during inference. This leads to more concise and interpretable explanations and reduces the risk of information leakage that arises from passing dense or uncertain embeddings [20, 21] directly to the classifier. To the best of our knowledge, this is the first instance of integrating uncertainty into the V-IP framework. In our approach, we first quantify both aleatoric and epistemic uncertainties for each query-answer. We then modify the V-IP framework to prioritize more informative queries by bypassing the uninformative ones, mimicking human-like decision-making. Experiments conducted on four diverse datasets including dermoscopic and ultrasound breast cancer, demonstrate that UAV-IP improves the performance of baseline V-IP models, and produces more meaningful interpretations, i.e., shorter explanations that do not include uncertain clinical concepts.

2 Methodology

2.1 Problem Definition and Preliminary

The *supervised query-based classification* scenario consists of two main components. First, given an input image $x \in \mathcal{X}$ ³, the task is to predict answers to a set of queries based on human-interpretable concepts. Each query, Q_m , is defined as a function $Q_m : \mathcal{X} \rightarrow \mathbb{Z}_2$, mapping input data x to a corresponding binary answer $q_m(x)$. For example, if x represents a dermoscopic image of skin and Q_m corresponds to the query “Does the lesion exhibit a typical pigment network?”, then $q_m(x)$ would be +1 for lesions exhibiting a typical pigment network and −1 otherwise. A collection of M such query functions is denoted by $\mathcal{Q} = \{Q_1, Q_2, \dots, Q_M\}$. Second, the goal is to predict the class label $y \in \mathcal{Y}$ for the image using the query-answer pairs generated in the previous step. We assume that these query-answer pairs are sufficient for solving the task, meaning that for all $(x, y) \in (\mathcal{X}, \mathcal{Y})$, the following holds: $P(y | x) = P(y | x' \in \mathcal{X} : \{q_m(x') = q_m(x)\}_{m=1}^M)$.

Variational Information Pursuit (V-IP): In the V-IP framework [13], the set of queries is defined by domain experts. Alternatively, large language models (LLMs) can be used to derive these concepts, offering a data-driven approach to query generation [22, 23, 24, 14]. The answers to the set of queries for a given test image are generated using a supervised deep neural network $Q_\theta : \mathcal{X} \rightarrow \mathbb{Z}_2^M$. The V-IP algorithm, which predicts the class label given the set of query-answer pairs, consists of two learnable components:

1. *Querier:* A sequential decision-making agent that selects the next most informative query, $Q_{t+1} \in \mathcal{Q}$ for a given image x , based on the history of observed query-answers $\mathcal{H}_{[1:t]} := \{Q_i, q_i(x)\}_{i=1:t} \in \mathbb{H}$. The querier is represented by the function $g_\gamma : \mathbb{H} \rightarrow \mathcal{Q}$.

¹For example, a query such as “Is typical pigment network” might be confidently predicted for one image (low uncertainty), but be highly ambiguous for another image due to low visual quality or occlusion (high uncertainty).

²The V-IP framework is capable of capturing *dataset-level uncertainties*—i.e., identifying queries that are generally more informative and reliable within the training distribution. However, it cannot handle *sample-level uncertainties*.

³Here, random variables are represented by uppercase while their specific realizations are denoted by lowercase letters.

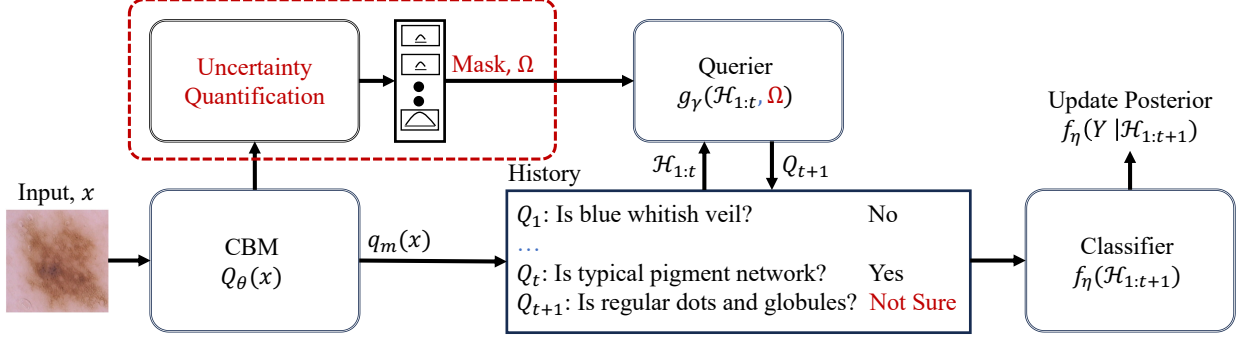


Figure 1: Overall V-IP framework with the proposed UAV-IP modifications highlighted in red. UAV-IP incorporates uncertainty quantification to help the querier skip low-confidence/high-uncertainty questions.

2. *Probabilistic Classifier*: Predicts the posterior $P(Y | q_{t+1}(x), \mathcal{H}_{[1:t]})$. The classifier is represented by the function $f_\eta : \mathbb{H} \rightarrow \mathcal{Y}$.

The parameters of the two learnable networks above are jointly learned by optimizing the following objective [13]:

$$\min_{\gamma, \eta} \mathbb{E}_{X, \mathcal{H}} [D_{\text{KL}}(P(Y | X) \| f_\eta(Y | g_\gamma(\mathcal{H}_{[1:t]}), \mathcal{H}_{[1:t]}))] . \quad (1)$$

During inference, the querier sequentially selects queries from \mathcal{Q} , until $f_\eta(Y | \mathcal{H}_{[1:t+1]})$ reaches a predefined threshold. The sequence of observed query answers, $\mathcal{H}_{[1:t+1]}$, at the point of termination constitutes the explanation.

2.2 Proposed Method

The V-IP framework described above relies on a CBM model, $Q_\theta(x)$, to provide accurate answers to the queries selected by the queried, g_γ . However, in real-world applications like medical imaging, almost no model achieves perfect accuracy. These inaccuracies in query answering can cause the querier to select less ideal queries, which may lead to incorrect predictions. To address this, we can draw inspiration from how human experts handle information in clinical decision-making. When an expert is faced with ambiguity in the result of a clinically relevant test – due to difficulty in determining the significance of the outcome or other causes of uncertainty – the expert may instead utilize other relevant but more reliable information to guide their decisions. Building on this intuition, *we hypothesize that uncertainty in the query answer generator, Q_θ , is correlated with the reliability of its output and incorporating this into the V-IP framework leads to a more robust interpretable-by-design (IBD) model.*

In our modified framework, termed Uncertainty-Aware Variational Information Pursuit (UAV-IP), the query-answer model not only predicts the presence or absence of a given concept but also quantifies uncertainty in the answer (i.e., “yes”, “no”, “not sure”). Consequently, UAV-IP refines the query selection process by prioritizing queries that are both reliable and informative when uncertainty is detected. The overall block diagram of UAV-IP is shown in Figure 1, and the following sections describe the steps for uncertainty quantification and the modified query selection process.

2.2.1 Query-Wise Uncertainty Quantification:

Multiple methods have been proposed in the literature to quantify uncertainty in deep learning models [25]. In this paper, we employ two commonly used uncertainty measures.

First, we use entropy, a widely adopted measure of uncertainty. We refer to this variant as *UAV-IP (Entropy)*. Given an input image x and a query Q_m , the concept model $Q_\theta(x)$ outputs a probability distribution on the labels, $\Phi^{(m)} \in \mathbb{P}(\mathcal{Y})$, where each element, $\phi_k^{(m)} = P(Y = y_k | x, \theta)$. Here, $k = \{+1, -1\}$ as our queries have binary outputs. The entropy-based uncertainty is computed as,

$$H(Q_m) = - \sum_{k \in \{-1, 1\}} \phi_k^{(m)} \log_2(\phi_k^{(m)}) . \quad (2)$$

Secondly, we employ a recent variant of the popular Monte Carlo dropout [26]. This approach (see Sale et al. [17]’s prior work for the full derivation) quantifies total uncertainty by analyzing the distribution of $\Phi^{(m)}$, denoted as

$\Pi^{(m)} \in \mathbb{P}(\mathbb{P}(\mathcal{Y}))$. Thus, we define total uncertainty of a query, m , as:

$$\text{TU}(Q_m) = \underbrace{\mathbb{E}_{\Phi^{(m)} \sim \Pi_m} \left[\Phi^{(m)} \left(1 - \Phi^{(m)} \right) \right]}_{\text{Aleatoric}} + \underbrace{\text{Var}_{\Phi^{(m)} \sim \Pi_m} \left(\Phi^{(m)} \right)}_{\text{Epistemic}}. \quad (3)$$

Using Monte Carlo samples from Π_m , the above can be estimated as:

$$\text{TU}(Q_m) = \frac{1}{|\mathcal{S}|} \sum_{s \in \mathcal{S}} \Phi_m^{(s)} \left(1 - \Phi_m^{(s)} \right) + \frac{1}{|\mathcal{S}|} \sum_{s \in \mathcal{S}} \left(\Phi_m^{(s)} - \bar{\Phi}_m \right)^2. \quad (4)$$

We employ the loss-based approach described in Sale et. al [17] to calculate the above measure and call this variant *UAV-IP (MonteCarlo)*.

Once the uncertainty is quantified using the above two methods, we use a threshold on uncertainties to derive a mask for each query m as follows:

$$\Omega_m(x) = \begin{cases} 1 & \mathcal{U}(Q_m) \geq \mathcal{T}_{\square} (\mathcal{T}_{MC} \text{ or } \mathcal{T}_E) \\ 0 & \mathcal{U}(Q_m) < \mathcal{T}_{\square} (\mathcal{T}_{MC} \text{ or } \mathcal{T}_E). \end{cases} \quad (5)$$

Here $\mathcal{U}(Q_m) = H(Q_m)$ for the UAV-IP (Entropy) and $\mathcal{U}(Q_m) = \text{TU}(Q_m)$ for UAV-IP (MonteCarlo). The thresholds \mathcal{T} for the two uncertainty estimation methods are chosen as follows. For UAV-IP (Entropy), we set the threshold to an empirically determined value of $\mathcal{T}_E = 0.95$ across all datasets. For UAV-IP (MonteCarlo), the threshold \mathcal{T}_{MC} is determined using a validation set. Specifically, we train a simple linear classifier (i.e., a single-threshold model) to distinguish between correct and incorrect query-answer pairs using the computed confidence scores as input and the ground-truth labels. This classifier enables us to determine an optimal threshold for \mathcal{T}_{MC} for each data set.

2.2.2 Modified Variational Information Pursuit (V-IP) for Uncertainty Handling:

As previously discussed, the original V-IP framework selects queries solely based on the expected informativeness of next possible queries learned on a data-set level, without accounting for the uncertainty of those query-answers on a sample-level (e.g.: a certain concept may be occluded in one particular image, leading to uncertain concept answers, which should be excluded from the decision making process). This can result in unreliable or ambiguous queries being included in the explanation, which negatively affects interpretability and decision reliability.

To address this, we modify the V-IP framework to include sample-level uncertainty into the querying process. Specifically, we modify the querier, g_γ , to select the next most informative query Q_{t+1} based on both the query-answer history $\mathcal{H}_{[1:t]}$ and the uncertainty mask Ω . *Unlike the original V-IP model where the querier considers only the query-answer history, our approach allows the querier to focus only on reliable information, leading to shorter and more interpretable explanations*, aligned with the original goal of V-IP achieving accurate predictions with minimal explanation length. The modified objective of the UAV-IP is given by:

$$\min_{\gamma, \eta} \mathbb{E}_{X, \mathcal{H}} \left[D_{\text{KL}} \left(P(Y | X) \parallel f_\eta \left(Y | g_\gamma \left(\mathcal{H}_{[1:t]}, \Omega \right), \mathcal{H}_{[1:t]} \right) \right) \right] \quad (6)$$

The masks, Ω , are computed sample-wise and do not require labels allowing the V-IP to handle sample-level uncertainties in both training and test data, on top of the existing capability to handle dataset-level uncertainties.

3 Experiments and Results

3.1 Experimental Setup:

In our experimental analysis, four datasets (PH2 [27], Derm7pt [28], BrEaST [29], and SkinCon [30]), are examined, each containing annotations for clinically relevant concepts. The PH2 dataset consists of 200 dermoscopic images, each with eight annotated clinical concepts, while Derm7pt contains 827 images with 38 annotated concepts. The BrEaST dataset includes 256 ultrasound images annotated with seven BI-RADS descriptors. SkinCon, derived from Fitzpatrick 17k, comprises 3,230 images with 48 densely annotated clinical concepts for this dataset, following prior work [11, 31], we selected a subset of 22 concepts with at least 50 images per concept to ensure high enough sample sizes for meaningful learning.

The proposed UAV-IP framework is trained in two stages: First, The CBM (i.e., ResNet101 backbone) was trained using concept labels. The concept labels and their associated uncertainty were then used to train the final predictor (i.e., Querier and the classifier). Throughout our experiments, we used the same parameter values and hyper-parameter settings as the original V-IP framework [13]. The Adam optimizer with a learning rate of $\text{lr} = 1e-4$ was used to train

Table 1: Comparative performance of different state-of-art models across four datasets. **Bold** indicates the best non-oracle result and P-values from the Wilcoxon signed-rank test highlight significant differences between UAV-IP (MonteCarlo) and other methods.

Dataset	Model	Accuracy \uparrow	AUC \uparrow	Queries \downarrow	F1 Score \uparrow	P-Value
Derm7pt	CBM (ICML 2020) [9]	82.01 \pm 1.27	87.60 \pm 2.68	38.00 \pm 0.00	79.91 \pm 2.21	< 0.001
	evi-CEM (MICCAI 2024) [20]	79.70 \pm 2.06	83.95 \pm 2.50	38.00 \pm 0.00	75.68 \pm 1.51	< 0.001
	V-IP (ICLR 2023) [13]	81.81 \pm 1.38	87.90 \pm 1.33	26.81 \pm 0.93	81.36 \pm 1.36	< 0.001
	UAV-IP (Entropy)	81.75 \pm 2.33	87.91 \pm 2.07	24.68 \pm 3.38	75.92 \pm 3.17	< 0.001
	UAV-IP (MonteCarlo)	83.49 \pm 1.26	89.99 \pm 1.49	23.65 \pm 0.52	77.11 \pm 2.13	-
	UAV-IP (Oracle)	92.29 \pm 1.70	97.18 \pm 0.64	18.44 \pm 0.86	92.07 \pm 1.79	-
SkinCon	CBM (ICML 2020) [9]	75.01 \pm 1.16	74.71 \pm 0.96	22.00 \pm 0.00	58.70 \pm 4.03	< 0.001
	evi-CEM (MICCAI 2024) [20]	75.36 \pm 1.28	75.87 \pm 2.54	22.00 \pm 0.00	45.14 \pm 1.42	< 0.001
	V-IP (ICLR 2023) [13]	74.77 \pm 0.28	65.26 \pm 0.91	17.89 \pm 0.45	67.39 \pm 0.57	< 0.001
	UAV-IP (Entropy)	75.75 \pm 0.79	73.19 \pm 0.57	18.20 \pm 0.14	64.80 \pm 1.26	< 0.001
	UAV-IP (MonteCarlo)	75.80 \pm 0.46	73.47 \pm 0.59	14.89 \pm 0.25	65.80 \pm 0.46	-
	UAV-IP (Oracle)	76.57 \pm 0.33	73.84 \pm 1.28	14.53 \pm 0.11	70.82 \pm 0.57	-
BrEaST	CBM (ICML 2020) [9]	85.88 \pm 4.22	91.10 \pm 3.20	7.00 \pm 0.00	83.72 \pm 4.28	< 0.001
	evi-CEM (MICCAI 2024) [20]	80.78 \pm 3.17	85.34 \pm 3.21	7.00 \pm 0.00	77.37 \pm 3.26	< 0.001
	V-IP (ICLR 2023) [13]	87.57 \pm 5.09	94.28 \pm 2.00	6.25 \pm 0.33	86.60 \pm 4.86	< 0.001
	UAV-IP (Entropy)	88.64 \pm 1.86	94.40 \pm 1.64	6.51 \pm 0.09	88.84 \pm 2.00	< 0.001
	UAV-IP (MonteCarlo)	88.14 \pm 3.97	95.05 \pm 2.29	6.57 \pm 0.05	88.14 \pm 4.06	-
	UAV-IP (Oracle)	89.44 \pm 4.36	95.98 \pm 1.79	6.20 \pm 0.10	89.56 \pm 4.30	-
PH2	CBM (ICML 2020) [9]	92.00 \pm 4.11	96.50 \pm 2.74	8.00 \pm 0.00	83.07 \pm 3.63	< 0.001
	evi-CEM (MICCAI 2024) [20]	90.50 \pm 3.26	93.77 \pm 3.79	8.00 \pm 0.00	75.90 \pm 4.93	< 0.001
	V-IP (ICLR 2023) [13]	88.00 \pm 4.47	89.77 \pm 4.88	7.96 \pm 0.02	88.10 \pm 4.07	0.02
	UAV-IP (Entropy)	91.30 \pm 3.21	93.75 \pm 4.20	6.13 \pm 0.28	86.59 \pm 6.11	< 0.001
	UAV-IP (MonteCarlo)	92.10 \pm 3.16	95.40 \pm 1.29	6.29 \pm 0.16	89.74 \pm 5.58	-
	UAV-IP (Oracle)	92.50 \pm 3.18	96.23 \pm 2.21	6.13 \pm 0.20	92.99 \pm 3.20	-

both the classifier and querier networks for 200 epochs. A batch size of 16 was used for PH2 and BrEaST datasets, and 64 was used for the larger Derm7pt and SkinCon. The temperature parameter τ in the straight-through softmax estimator was linearly annealed from 1.0 to 0.2 throughout training. All experiments were implemented in PyTorch, and executed on Kaggle with a Tesla P100 GPU (13 GB VRAM) and 26 GB system RAM.

3.2 Experimental Results:

The results of the proposed method for the above four datasets are shown in Table 1. Each method is run 10 times with random training-validation-test data splits and seeds, reporting the mean and standard deviation. Alongside the two UAV-IP variants (Entropy and MonteCarlo), we include an oracle-based approach, UAV-IP(Oracle), that uses ground truth labels to generate the uncertainty mask to provide an upper-performance bound on masking inaccurate queries (i.e., if the ground truth answer for a query is different from the predicted answer by CBM, Q_θ , then that answer is deemed uncertain). While useful for analysis, it is impractical in real-world settings where concept labels are unavailable for test samples. In summary, results show that incorporating uncertainty leads to superior performance while requiring fewer queries. Additionally, UAV-IP (MonteCarlo) performs closely to UAV-IP(Oracle), indicating that further improvements in the accuracy of uncertainty estimations would yield minimal gains.

The original V-IP learns to select the next query based solely on the current set of query answers, including those that are uncertain or incorrect, regardless of the current sample, which may result in inaccurate confidence levels and predictions. To counter this, the model may learn to ask more queries in order to become more certain: for example, in the PH2 dataset, V-IP requires all 8 queries to reach an accuracy of 88.00 ± 4.47 , and it requires 27 queries in the Derm7pt dataset to achieve an accuracy of 81.81 ± 1.38 . On the other hand, UAV-IP (MonteCarlo), achieves more accurate predictions with significantly fewer queries by skipping uncertain queries. For the PH2 dataset, it achieves an accuracy of 92.10 ± 3.16 using only six queries on average, while in the Derm7pt dataset, it achieves 83.49 ± 1.26 using just 23 queries. Beyond comparisons with V-IP-based methods, we further benchmark against CBM [9] and

its uncertainty-aware extension, evi-CEM [20]. Notably, UAV-IP (MonteCarlo) demonstrates superior performance over both across all evaluated datasets. The superior performance of UAV-IP (MonteCarlo) is likely due to its explicit uncertainty handling, which is essential in medical datasets prone to noise, variability, and data limitations. In contrast, both CBM and evi-CEM rely on the full spectrum of concept predictions, including those with high uncertainty or incorrect outputs. Such indiscriminate usage compromises the reliability of their explanations and may yield misleading inferences that posing significant risks in safety-critical domains such as healthcare.

3.3 Discussion:

Here, we analyze the factors contributing to the improvements of our proposed method over the baseline V-IP. Our central hypothesis, *incorporating uncertainty into the V-IP framework enhances performance*, hinges on two sub parts: 1) Uncertainty serves as an effective measure for determining instances where the CBM makes incorrect predictions, 2) Filtering out incorrect query-answer predictions leads to overall improved performance. To validate these hypotheses, we first evaluated the ability of uncertainty estimation to classify whether a given query-answer is correct, using ground-truth annotations as a reference. The average AUC values across four datasets, shown in Table 2, indicate that both uncertainty measures exhibit reasonable predictive power in detecting incorrect query-answers. Notably, second-order Monte Carlo-based uncertainty estimates outperform entropy-based estimates in this task. Next, we analyzed the impact of filtering incorrect answers using uncertainty estimates. Table 1 shows that leveraging uncertainty improves accuracy and explanation clarity over V-IP. Additionally, we grouped test samples by incorrect query-answer count and calculated average accuracy for each group. Our results for the BrEaST dataset, shown in figure 2, indicate that when CBM predictions are mostly correct, V-IP performs comparably to both UAV-IP (MonteCarlo) and the oracle. However, as the number of incorrect query-answers increases (≥ 2), UAV-IP significantly outperforms V-IP, achieving accuracy levels comparable to the oracle. Similar results were observed in the other three datasets but were not included here due to space limitations. These findings highlight the effectiveness of integrating uncertainty into the V-IP framework, showing that uncertainty-aware filtering improves both accuracy and explanation reliability.

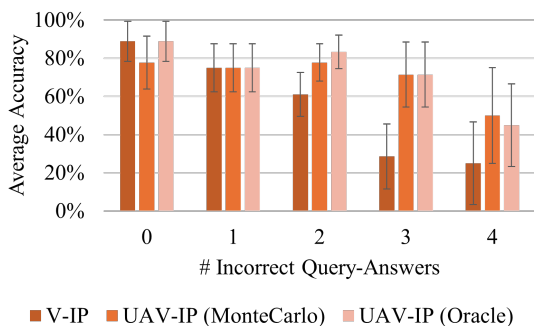


Figure 2: Relationship between accuracy and the number of incorrect query-answer predictions made by CBM on the BrEaST dataset.

Table 2: The effectiveness of uncertainty estimates in classifying query-answer correctness, measured by average AUC using ground-truth annotations.

Dataset	MonteCarlo	Entropy
PH2	95.75%	91.19%
Derm7pt	84.59%	74.64%
BrEaST	91.00%	71.30%
Skincon	92.28%	89.60%

4 Conclusion

In this work, we introduced the first integration of uncertainty quantification into an IBD model by extending the V-IP framework. By measuring uncertainty in the concept model’s answers, our proposed UAV-IP improves query selection in a simple but effective manner, by ignoring uncertain queries leading to increased accuracy and more concise explanations. By bridging the gap between interpretability and uncertainty handling, this improvement makes it possible to arrive at more trustworthy decisions in query-based classification. A major limitation of the V-IP framework is its reliance on annotated concept training datasets. This has already been addressed in other works using LLMs and VLMs [14]. As such, we aim to quantify uncertainty in LLMs and VLMs, allowing them to generate and answer queries with uncertainty. Additionally, we explore better ways to handle ambiguous questions instead of ignoring them, as they may contain valuable information.

References

- [1] Davide Castelvecchi. Can we open the black box of ai? *Nature News*, 538(7623):20, 2016.

- [2] Ravid Shwartz-Ziv and Naftali Tishby. Opening the black box of deep neural networks via information. *Information Flow in Deep Neural Networks*, page 24, 2022.
- [3] Aditya Chattopadhyay, Anirban Sarkar, Prantik Howlader, and Vineeth N Balasubramanian. Grad-cam++: Generalized gradient-based visual explanations for deep convolutional networks. In *2018 IEEE winter conference on applications of computer vision (WACV)*, pages 839–847. IEEE, 2018.
- [4] Ramprasaath R Selvaraju, Michael Cogswell, Abhishek Das, Ramakrishna Vedantam, Devi Parikh, and Dhruv Batra. Grad-cam: Visual explanations from deep networks via gradient-based localization. In *Proceedings of the IEEE international conference on computer vision*, pages 618–626, 2017.
- [5] Matthew D Zeiler and Rob Fergus. Visualizing and understanding convolutional networks. In *Computer Vision–ECCV 2014: 13th European Conference, Zurich, Switzerland, September 6–12, 2014, Proceedings, Part I 13*, pages 818–833. Springer, 2014.
- [6] Marco Tulio Ribeiro, Sameer Singh, and Carlos Guestrin. " why should i trust you?" explaining the predictions of any classifier. In *Proceedings of the 22nd ACM SIGKDD international conference on knowledge discovery and data mining*, pages 1135–1144, 2016.
- [7] Cynthia Rudin. Stop explaining black box machine learning models for high stakes decisions and use interpretable models instead. *Nature machine intelligence*, 1(5):206–215, 2019.
- [8] Julius Adebayo, Justin Gilmer, Michael Muelly, Ian Goodfellow, Moritz Hardt, and Been Kim. Sanity checks for saliency maps. *Advances in neural information processing systems*, 31, 2018.
- [9] Pang Wei Koh, Thao Nguyen, Yew Siang Tang, Stephen Mussmann, Emma Pierson, Been Kim, and Percy Liang. Concept bottleneck models. In *International conference on machine learning*, pages 5338–5348. PMLR, 2020.
- [10] Sandareka Wickramanayake, Wynne Hsu, and Mong Li Lee. Comprehensible convolutional neural networks via guided concept learning. In *2021 International Joint Conference on Neural Networks (IJCNN)*, pages 1–8. IEEE, 2021.
- [11] Cristiano Patrício, João C Neves, and Luis F Teixeira. Coherent concept-based explanations in medical image and its application to skin lesion diagnosis. In *Proceedings of the IEEE/CVF Conference on Computer Vision and Pattern Recognition*, pages 3799–3808, 2023.
- [12] Aditya Chattopadhyay, Stewart Slocum, Benjamin D Haeffele, Rene Vidal, and Donald Geman. Interpretable by design: Learning predictors by composing interpretable queries. *IEEE Transactions on Pattern Analysis and Machine Intelligence*, 45(6):7430–7443, 2022.
- [13] Aditya Chattopadhyay, Kwan Ho Ryan Chan, Benjamin David Haeffele, Donald Geman, and Rene Vidal. Variational information pursuit for interpretable predictions. In *The Eleventh International Conference on Learning Representations*, 2023.
- [14] Aditya Chattopadhyay, Kwan Ho Ryan Chan, and Rene Vidal. Bootstrapping variational information pursuit with large language and vision models for interpretable image classification. In *The Twelfth International Conference on Learning Representations*, 2024.
- [15] Donald Geman and Bruno Jedynak. An active testing model for tracking roads in satellite images. *IEEE Transactions on Pattern Analysis and Machine Intelligence*, 18(1):1–14, 1996.
- [16] Eyke Hüllermeier and Willem Waegeman. Aleatoric and epistemic uncertainty in machine learning: An introduction to concepts and methods. *Machine learning*, 110(3):457–506, 2021.
- [17] Yusuf Sale, Paul Hofman, Timo Löhr, Lisa Wimmer, Thomas Nagler, and Eyke Hüllermeier. Label-wise aleatoric and epistemic uncertainty quantification. In *The 40th Conference on Uncertainty in Artificial Intelligence*, 2024.
- [18] Junjia Huang, Chenming Shang, Aolin Xiong, Yuxian Pang, and Zhi Jin. Seeing health with eyes: Feature combination for image-based human bmi estimation. In *2021 IEEE International Conference on Multimedia and Expo (ICME)*, pages 1–6. IEEE, 2021.
- [19] Ruxiao Duan, Brian Caffo, Harrison X Bai, Haris I Sair, and Craig Jones. Evidential uncertainty quantification: A variance-based perspective. In *Proceedings of the IEEE/CVF Winter Conference on Applications of Computer Vision*, pages 2132–2141, 2024.
- [20] Yibo Gao, Zheyao Gao, Xin Gao, Yuanye Liu, Bomin Wang, and Xiahai Zhuang. Evidential concept embedding models: Towards reliable concept explanations for skin disease diagnosis. In *International Conference on Medical Image Computing and Computer-Assisted Intervention*, pages 308–317. Springer, 2024.
- [21] Eunji Kim, Dahuin Jung, Sangha Park, Siwon Kim, and Sungroh Yoon. Probabilistic concept bottleneck models. In *International Conference on Machine Learning*, pages 16521–16540. PMLR, 2023.

- [22] Alec Radford, Jong Wook Kim, Chris Hallacy, Aditya Ramesh, Gabriel Goh, Sandhini Agarwal, Girish Sastry, Amanda Askell, Pamela Mishkin, Jack Clark, et al. Learning transferable visual models from natural language supervision. In *International conference on machine learning*, pages 8748–8763. PMLR, 2021.
- [23] Tuomas Oikarinen, Subhro Das, Lam M Nguyen, and Tsui-Wei Weng. Label-free concept bottleneck models. In *The Eleventh International Conference on Learning Representations*, 2023.
- [24] Yue Yang, Artemis Panagopoulou, Shenghao Zhou, Daniel Jin, Chris Callison-Burch, and Mark Yatskar. Language in a bottle: Language model guided concept bottlenecks for interpretable image classification. In *Proceedings of the IEEE/CVF Conference on Computer Vision and Pattern Recognition*, pages 19187–19197, 2023.
- [25] Jakob Gawlikowski, Cedrique Rovile Njiteutcheu Tassi, Mohsin Ali, Jongseok Lee, Matthias Humt, Jianxiang Feng, Anna Kruspe, Rudolph Triebel, Peter Jung, Ribana Roscher, et al. A survey of uncertainty in deep neural networks. *Artificial Intelligence Review*, 56(Suppl 1):1513–1589, 2023.
- [26] Yarin Gal and Zoubin Ghahramani. Dropout as a bayesian approximation: Representing model uncertainty in deep learning. In *international conference on machine learning*, pages 1050–1059. PMLR, 2016.
- [27] Teresa Mendonça, Pedro M Ferreira, Jorge S Marques, André RS Marcal, and Jorge Rozeira. Ph 2-a dermoscopic image database for research and benchmarking. In *2013 35th annual international conference of the IEEE engineering in medicine and biology society (EMBC)*, pages 5437–5440. IEEE, 2013.
- [28] Jeremy Kawahara, Sara Daneshvar, Giuseppe Argenziano, and Ghassan Hamarneh. Seven-point checklist and skin lesion classification using multitask multimodal neural nets. *IEEE journal of biomedical and health informatics*, 23(2):538–546, 2018.
- [29] Anna Pawłowska, Anna Ćwierz-Pieńkowska, Agnieszka Domalik, Dominika Jaguś, Piotr Kasprzak, Rafał Matkowski, Łukasz Fura, Andrzej Nowicki, and Norbert Żolek. Curated benchmark dataset for ultrasound based breast lesion analysis. *Scientific Data*, 11(1):148, 2024.
- [30] Roxana Daneshjou, Mert Yuksekogul, Zhuo Ran Cai, Roberto Novoa, and James Y Zou. Skincon: A skin disease dataset densely annotated by domain experts for fine-grained debugging and analysis. *Advances in Neural Information Processing Systems*, 35:18157–18167, 2022.
- [31] Hongmei Wang, Junlin Hou, and Hao Chen. Concept complement bottleneck model for interpretable medical image diagnosis. *arXiv preprint arXiv:2410.15446*, 2024.